Verification analysis of the MERCURY code for contact and friction models

Dong-Hwa Lee *, Sung Uk Lee, Hyo Chan Kim
LWR Fuel Technology Research Division, Korea Atomic Energy Research Institute,
111 Daedeok-Daero 989 Beon-gil, Yuseong-gu, Daejeon, Korea
**Corresponding author: donghwalee@kaeri.re.kr*

***Keywords :** FEM, contact analysis, friction analysis, MERCURY, fuel performance code

1. Introduction

To improve the economic competitiveness of nuclear power plants, flexible operation and high-burnup operation are receiving increasing consideration. Both operating modes heighten the need for dependable fuel performance assessment of pellet-cladding mechanical interaction (PCMI) and the associated risk of pellet-cladding interaction (PCI) failure [1].

For PCI failure to occur during a power transient, three conditions must be met simultaneously: sufficient cladding hoop stress generated by pellet thermal expansion, aggressive fission products such as iodine, and a susceptible cladding microstructure [2]. At low power, the gap reopens while coolant overpressure drives the cladding to creep inward; consequently, the next power increase imposes greater mechanical loading than in the previously conditioned state. Thus, frequent power changes accelerate de-conditioning and diminish the PCI margin.

The mechanical mechanism underlying PCI is PCMI. Contact between the thermally expanding pellet and the cladding is greatest at the pellet end faces, where geometric stress concentration produces the primary ridge. Evaluating these localized concentrations requires large mesh deformation, deformable-to-deformable contact, and nonlinear constitutive behavior; conventional 1.5D codes such as FRAPCON do not fully provide these capabilities [3]. The present study implemented nonlinear contact and friction models in MERCURY [4,5] and verified them using five analytical contact solutions.

2. Contact and friction models

Developed by KAERI, MERCURY (Multi-dimensional Entire fuel Rod Code for Understanding Reaction Yield behaviors) is an FEM-based fuel performance code for multidimensional thermo-mechanical analysis of LWR fuel rods [4,5]. It was developed under the institute's software quality assurance (SQA) procedure and has been validated through out-of-pile and in-pile LOCA tests [6]. In this work, it is augmented by a penalty-method-based node-to-segment (NTS) contact algorithm, and a regularized Coulomb friction model, based on 8-node axisymmetric element.

At the interface, the normal gap g_N characterizes the kinematic state and is obtained by projecting the relative displacement of the candidate contact points onto the local normal direction [7]. Non-penetration and the normal traction t_N are jointly represented by the complementarity condition

$$g_N \geq 0,\ t_N \leq 0,\ g_N \cdot t_N = 0 \quad (1)$$

whereas the sliding gap g_T and the tangential traction t_T satisfy the Coulomb law,

$$|t_T| \leq \mu |t_N| \quad (2)$$

where μ denotes the friction coefficient; strict inequality identifies stick, and equality identifies slip. To impose these constraints, the penalty method places a virtual spring between the surfaces and incorporates the contact contribution directly into the global stiffness matrix without introducing additional unknowns [7]. For the penetrated state,

$$t_N = k_N \cdot g_N,\ (g_N < 0) \quad (3)$$

and the tangential traction is obtained from the trial value $k_T g_T$ through the regularized Coulomb law of Eq. (4). Scaling both penalty stiffnesses by the elastic modulus, as $k_N = \alpha E$ and $k_T = \beta E$, makes constraint enforcement nearly insensitive to the absolute material stiffness.

Under the NTS discretization [8], every slave node is projected onto a quadratic isoparametric master segment specified by three nodes, with the contact point ξ^* determined by minimizing the squared distance function. Shape functions distribute the resulting force from the slave node among the three master nodes, while the consistent contact tangent maintains quadratic Newton-Raphson convergence [9].

Imposed as a discontinuous switch, the stick-slip transition would make the tangential stiffness discontinuous and provoke divergence at intermediate friction. The law is therefore regularized as

$$q = \mu \cdot p \tanh\left(\frac{q_{trial}}{\mu \cdot p}\right) \quad (4)$$

which remains continuously differentiable while reproducing the exact Coulomb law in the stick and slip limits. As the slip fraction increases, an anchor-blending strategy pulls the stick reference point toward the current contact point.

3. Verification

Using axisymmetric 8-node elements, five problems having closed-form solutions were examined: (I) Hertz contact between a rigid sphere and an elastic half-space

[10], (II) contact between two identical deformable spheres, (III) flat-punch indentation with a singular pressure field (Sneddon's problem) [11], (IV) Spence's problem [12], which combines Coulomb friction and a Poisson-ratio mismatch, and (V) sequential contact of three concentric cylinders undergoing thermal expansion. The results are summarized in Table I.

Table I. Summary of the verification results.

Case	Quantity	Analytic	MERCURY	Error
Hertz	F [N]	1035.95	1037.25	0.13 %
Hertz	p_0 [GPa]	98.93	97.57	1.37 %
Two spheres	F [N]	1036.05	1038.61	0.25 %
Two spheres	p_0 [GPa]	98.93	96.28	2.68 %
Flat punch	F [N]	1035.95	1038.42	0.24 %
Flat punch	p_0 [MPa]	659.5	660.8	0.19 %
Spence	F [N]	1182.0	1183.36	0.11 %
Three-body	p_{12} [MPa]	64.95	64.71	0.37 %
Three-body	p_{23} [MPa]	16.35	16.08	1.68 %

For every case, global force equilibrium is matched within 0.4%, and the representative contact pressure is reproduced within 3%. Increasing the Hertz mesh from 26,371 to 94,462 nodes altered the results by less than 0.1%. Apart from the discretization-induced edge artifact at $r/a = 1$, the calculated profile shows good agreement with the analytic curve, as shown in Fig. 1.

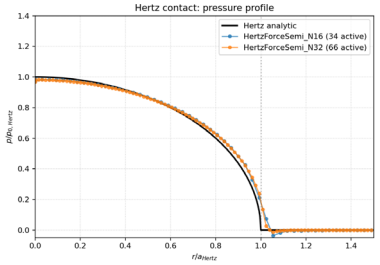


Fig. 1. Hertz axisymmetric contact: MERCURY pressure profile compared with the analytic Hertz solution.

For Spence's problem, the force accuracy is 0.11% at $\mu = 0$, 0.3 and 1.0, demonstrating that the normal solution remains unaffected by friction. Meanwhile, the frictional cases exhibit the higher local pressure predicted by Spence, see Fig. 2. With $\mu = 0.3$, a partial-slip annulus develops, comprising 14 nodes in stick and 19 in slip and having a stick radius $r_{stick}/a = 0.99$.

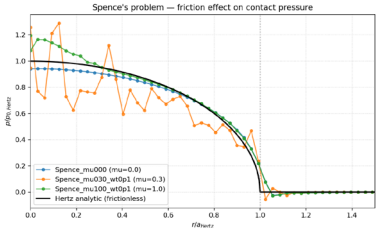


Fig. 2. Spence's problem: contact pressure profiles for three friction levels.

4. Conclusions

MERCURY was equipped with nonlinear contact and friction capabilities. Large PCMI deformation is accommodated by an 8-node axisymmetric element using a Total Lagrangian formulation, while a penalty-based NTS algorithm evaluates pellet-pellet and pellet-cladding contact. A tanh-regularized Coulomb model supplies continuous tangential stiffness through the stick-slip threshold, thereby ensuring stable convergence from frictionless to near-bonded conditions.

The five analytical benchmarks were matched within 0.4% for force equilibrium and 2-3% for contact pressure. Because both surfaces in the two-sphere case are curved and deform concurrently, that case demonstrates the correct re-projection of slave nodes onto an evolving master segment by the NTS routine. The three-body case additionally verifies consistent coupling with thermal expansion.

ACKNOWLEDGEMENT

This work was supported by the Korea Institute of Energy Technology Evaluation and Planning (KETEP) and the Ministry of Climate, Energy & Environment (MCEE) of the Republic of Korea (RS-2025-16852968).

REFERENCES

[1] IAEA, Non-baseload Operation in Nuclear Power Plants: Load Following and Frequency Control Modes of Flexible Operation, IAEA-NES NP-T-3.23, 2018.
[2] B. Cox, Pellet-clad interaction (PCI) failures of zirconium alloy fuel cladding - A review, J. Nucl. Mater., vol. 172, pp. 249-292, 1990.
[3] K. J. Geelhood, et al., FRAPCON-4.0: A Computer Code for the Calculation of Steady-State, Thermal-Mechanical Behavior of Oxide Fuel Rods for High Burnup, PNNL-19418, Vol.1 Rev.2, 2015.
[4] H. C. Kim, et al., Development of MERCURY for simulation of multidimensional fuel behavior for LOCA condition, Nucl. Eng. Des., vol. 369, 110853, 2020.
[5] H. C. Kim, et al., MERCURY V1.0 Theory Manual, KAERI/TR-10442/2024, 2024.
[6] S. U. Lee, et al., Validation of MERCURY code under LOCA condition with out-of-pile and in-pile tests, Nucl. Eng. Des., vol. 392, 111775, 2022.
[7] P. Wriggers, Computational Contact Mechanics, 2nd ed., Springer-Verlag, Berlin, 2006.
[8] J. O. Hallquist, et al., Sliding interfaces with contact-impact in large-scale Lagrangian computations, Comput. Methods Appl. Mech. Engrg., 51, pp. 107-137, 1985.
[9] K. J. Bathe, Finite Element Procedures, Prentice-Hall, Englewood Cliffs, 1996.
[10] K. L. Johnson, Contact Mechanics, Cambridge University Press, Cambridge, 1985.
[11] I. N. Sneddon, The relation between load and penetration in the axisymmetric Boussinesq problem for a punch of arbitrary profile, Int. J. Eng. Sci., vol. 3, pp. 47-57, 1965.
[12] D. A. Spence, The Hertz contact problem with finite friction, J. Elast., vol. 5, pp. 297-319, 1975.